

The effect of an activation solution with siliceous species on the chemical reactivity and mechanical properties of geopolymers

A. Gharzouni · E. Joussein · B. Samet ·
S. Baklouti · S. Pronier · I. Sobrados ·
J. Sanz · S. Rossignol

Received: 21 May 2014 / Accepted: 24 September 2014 / Published online: 2 October 2014
© Springer Science+Business Media New York 2014

Abstract Precursors are critical parameters in geopolymerization mechanisms because they govern the reaction kinetics as well as the working properties of the final materials. This study focuses on the effect of alkaline solutions on geopolymer formation. Toward this end, several geopolymer samples were synthesized from the same metakaolin and various alkaline solutions. First, the solutions were characterized by thermogravimetric analysis as well as DTA–TGA, infrared spectroscopy, and MAS-NMR spectrometry. The structural evolution of the formed geopolymers was investigated using infrared spectroscopy. The measurement of mechanical strength was tested by compression. The results provide evidence of relationships between the chemical composition, the extent of depolymerization of the alkaline solutions, the kinetics of Si–O–Si bond substitution by Si–O–Al and the compressive

strength. For a given aluminosilicate source, the nature and the quantity of siliceous species in the activation solution appear to lead to variation in the reactivity and, consequently, to the formation of various networks that control the kinetics of formation of geopolymers and their mechanical properties.

Keywords Si/K ratio · Alkaline solution · Depolymerization · Siliceous species · ^{29}Si MAS-NMR · TEM

1 Introduction

The development of new economical construction materials with low energy consumption and good environmental compatibility remains a current global challenge. Geopolymer materials have garnered increasing interest because of their synthesis methods, high working performance [1], wide range of applications [2] and low environmental impact [3]. Their properties make them a promising alternative to ordinary Portland cement. Geopolymer binders are amorphous, three-dimensional materials that result from the activation of an aluminosilicate source, such as metakaolin, calcined clay or industrial waste activated by an alkaline solution at a temperature less than 100 °C [4]. The choice of precursors is a critical parameter in geopolymerization mechanisms because it governs the properties of the final materials.

The role of aluminosilicate precursors has been extensively studied. Previous studies have focused on the nature of the raw materials, the influence of the impurities [5] and the effect of the calcination temperature [6]. Metakaolin is the most commonly used raw material because of its high reactivity and purity [7]. Recently, Autef et al. [8] studied

A. Gharzouni · S. Rossignol (✉)
Sciences des Procédés Céramiques et Traitements de Surface
(SPCTS), Ecole Nationale Supérieure de Céramique Industrielle,
12 rue Atlantis, 87068 Limoges Cedex, France
e-mail: sylvie.rossignol@unilim.fr

A. Gharzouni · B. Samet · S. Baklouti
Laboratoire de Chimie Industrielle, Ecole Nationale d'Ingénieurs
de Sfax, 3038 Sfax, Tunisie

E. Joussein
Université de Limoges, GRESE EA 4330, 123 Avenue Albert
Thomas, 87060 Limoges, France

S. Pronier
IC2MP, 40 Avenue du recteur Pineau, 86022 Poitiers, France

I. Sobrados · J. Sanz
Instituto de Ciencia de Materiales de Madrid, Consejo Superior
de Investigaciones Científicas (CSIC), C/Sor Juana Inés de la
Cruz, 3, 28049 Madrid, Spain

different Metakaolin in terms of reactivity, dehydroxylation process, amount of impurities have proposed a model of material formation based on the properties of the metakaolin used. Their model highlights the role of metakaolin reactivity in the presence of an alkaline solution, where this activity leads to the formation of one or more networks. These nanostructure variations influence the mechanical properties of the obtained materials.

The activating solution has been the subject of several studies. The nature of the alkali cation affects the geopolymerization reaction and the working properties of the consolidated materials. Geopolymers based on potassium exhibit better thermal and mechanical properties because of the larger size of the potassium ion compared to that of the sodium ion [9]. The concentration of silicon in the activating solution (the Si/M⁺ ratio, where M⁺ = Na⁺, K⁺, ...) plays an important role in the incorporation of alumina into the matrix [10].

Elucidation of the interaction of the alkaline solution with the aluminosilicate source requires that the structure of the silicate solution be defined. These products are manufactured by fusing silica with an alkali carbonate or sulfate at high temperatures. They have been widely studied; however, their chemistry has remained complex because of the variety of oligomeric silicate anion forms (monomer, linear, cyclic, prismatic, etc.) [11]. Infrared and ²⁹Si nuclear magnetic resonance spectroscopies (MAS NMR) contribute to the elucidation of the structure of silicate solutions. The structure is traditionally described with the notation Qⁿ [12] where Q represents the silicon atom coordinated to n bridging oxygen atoms and (4-n) non-bridging oxygen atoms in a tetrahedral environment.

Previous reports have demonstrated the existence of correlations between infrared wavenumber values and the Qⁿ units. Numerous infrared studies [13, 14] on silicate solutions have shown that bands located at approximately 1,060, 1080 and 1,165 cm⁻¹ are attributable to the Si–O–Si asymmetric stretching generated by Q², Q³ and Q⁴ units, respectively.

Even if the aluminosilicate structure is understood, data concerning the role and reactivity of the silica alkaline solution in geopolymer synthesis is lacking. The aim of this work was to analyze five alkaline compositions based on different commercial silicate solutions with different initial Si/K molar ratios and to investigate their influence on the properties of the synthesized geopolymers.

2 Experimental

2.1 Sample preparation

Five commercial potassium silicate solutions supplied by Woellner[®] were denoted as S0, S1, S2, S3 and S4 and were

Table 1 Nomenclature and characteristics of raw materials

Potassium silicate solutions		
Nomenclature	Si/K	Si/H ₂ O
S0	1.56	0.05
S1	1.75	0.05
S2	1.52	0.09
S3	0.67	0.09
S4	0.45	0.10

used as starting solutions. Table 1 details the Si/K and Si/H₂O molar ratios of each solution.

Because a comparison of solutions with different parameters is difficult, the Si/K molar ratio of the five solutions was maintained at Si/K = 0.5. To maintain the Si/K ratios, we dissolved different amounts of potassium hydroxide pellets (VWR, 85.2 % pure) into the S0, S1, S2 and S3 solutions. For S4 solution, very fine and highly reactive amorphous silica (Aldrich, 99.9 % pure) was dissolved into the solution to increase the concentration of Si because of its low Si/K ratio (Si/K = 0.45). The obtained modified alkaline solutions were denoted S_m0, S_m1, S_m2, S_m3 and S_m4. Metakaolin M-1000, supplied by Imerys[®] and composed of 55 wt% SiO₂, 40 wt% Al₂O₃, 0.8 wt% (K₂O + Na₂O), 1.4 wt% Fe₂O₃, 1.5 wt% TiO₂ and 0.3 wt% (CaO + MgO), was used as aluminosilicate source. Syntheses were performed by mixing the metakaolin and the five modified alkaline solutions until obtaining homogenous geopolymer reactive mixtures. The compositions of the different mixtures are reported in Table 2. Then, samples were placed in cylindrical closed sealable polystyrene molds at room temperature (25 °C) for 7 days. The synthesized geopolymer materials were denoted as G0, G1, G2, G3 and G4.

2.2 Characterization

To characterize the starting and modified silicate solutions, differential thermal analyses (DTA) and thermogravimetric analyses (TGA) were performed in platinum crucibles using an SDT Q600 apparatus from TA Instruments in an atmosphere of flowing dry air (100 mL/min). The signals were measured with Pt/Pt-10 % Rh thermocouples. The different solutions were heated to 350 °C at a rate of 5 °C/min.

FTIR spectra were obtained on a Thermo Fisher Scientific 380 infrared spectrometer (Nicolet) using the attenuated total reflection (ATR) method. The IR spectra were recorded over a range of 400–4,000 cm⁻¹ with a resolution of 4 cm⁻¹. The atmospheric CO₂ contribution was removed via a straight-line fit between 2,400 and 2,280 cm⁻¹. To monitor the geopolymer formation (G samples), software was used to acquire a spectrum (64

Table 2 Nomenclature and composition of the different prepared mixtures

Mixtures	Silicate solutions	KOH (wt%)	SiO ₂ (wt%)	MK (wt%)	(Si*H ₂ O)/(K + Al)	
G0	S0	50.7	10.3	–	39.0	0.81
G1	S1	50.7	10.3	–	39.0	0.83
G2	S2	48.4	14.4	–	37.2	0.71
G3	S3	53.7	5.1	–	41.3	0.68
G4	S4	55.6	–	1.6	42.8	0.64

scans) every 10 min for 13 h. For comparison, spectra were baseline corrected and normalized [15].

High-resolution MAS-NMR experiments were performed at room temperature on a Bruker AVANCE-400 spectrometer operating at 79.49 MHz (²⁹Si signal). The ²⁹Si (I = 1/2) MAS-NMR spectra were recorded after a $\pi/2$ -pulse irradiation (4 μ s) using a 500 kHz filter to improve the signal/noise ratio. In each case, 400 scans were collected. The time between acquisitions was set to 10 s to minimize saturation effects.

Compressive strengths were tested using a LLOYD EZ20 universal testing machine with a crosshead speed of 0.1 mm/min. The compressive tests were performed on ten

samples for each composition. The values of compressive strength represent the average of the ten obtained values and are expressed in MPa. Test tubes used for the compression tests were cylindrical in shape with a diameter (Φ) of 15 mm and a height (h) of approximately 35 mm [16] and were aged for 7 days in a closed mold at room temperature.

Finally, the morphology and chemical composition of each phase of two representative geopolymer samples were characterized by transmission electron microscopy (TEM) using a TEM/STEM JEOL 2100 UHR microscope operated at 200 kV. The elementary particle composition was determined by energy-dispersive X-ray analysis (EDX). Samples were deposited onto a Cu grid.

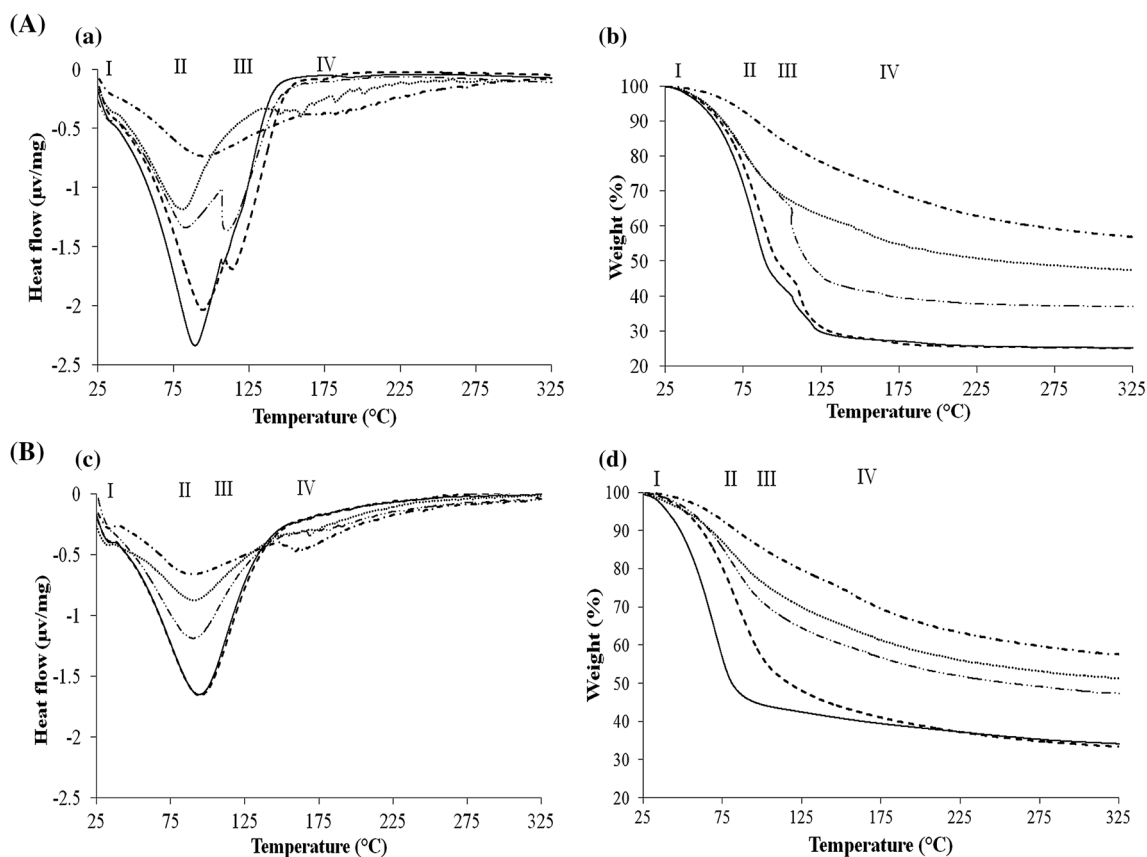


Fig. 1 DTA (a, c)–TGA (b, d) curves of (A) (dashed line) S0, (solid line) S1, (line with double filled circle) S2, (filled circle) S3 and (line with single filled circle) S4 starting solutions and (B) (solid line) S_m0,

(dashed line) S_m1, (line with double filled circle) S_m2, (filled circle) S_m3 and (line with single filled circle) S_m4 modified solutions

3 Results and discussion

3.1 Characterization of alkaline silicate solutions

3.1.1 Starting solutions

A preliminary characterization was performed using thermal analyses, infrared spectroscopy and ^{29}Si MAS-NMR to compare the starting silicate solutions used. Figure 1A (a, b) present the heat flow and the weight loss of the five solutions (S0–S4) as a function of temperature from 25 to 325 °C. The perturbations of the heat-flow signal observed at approximately 125 °C do not indicate that the obtained signals are not representative of the samples because they are characteristic of phenomena caused by the ebullition of the solution [17].

Irrespective of the solution, several endothermic peaks at varying temperatures less than 200 °C are observed. In the case of S0, the first two peaks at approximately 40 °C (I) and 95 °C (II) correspond to a relatively high weight loss (56.7 %), which is attributed to the elimination of free and physically adsorbed water [18]. The third peak at 114 °C (III), which is associated with a smaller weight loss (14.9 %), is related primarily to the release of constitutional water. The fourth peak at 175 °C (IV) corresponds to a weight loss of 3.4 %, which may be due to reactions in the ionic liquid between the oligomers [19]. The S1 solution exhibited similar heat-flow and weight-loss profiles, which indicates that S0 and S1 have similar structures. This result was expected because the two solutions have the same Si/K molar ratio.

In the case of the S2 solution, the same phenomena are observed. The main difference is that the third endothermic peak is more pronounced and is accompanied by a greater weight loss (18.3 %). This greater weight loss can be explained by the size of the anions present in the solution, which is intimately linked to the concentration of Si, as previously demonstrated in the literature [20]. Indeed, S2 has a lower Si/K ratio and a higher concentration of Si compared to S1 and S0, which results in a greater average colloidal species. Thus, water can be easily trapped in the structure. This phenomenon is observed less often for S3 and S4 solutions, revealing that these solutions contain smaller species than the S0, S1 and S2 solutions. This hypothesis remains to be confirmed by ^{29}Si NMR.

Furthermore, differences were detected in the amount of water in the starting solutions. The water content, as evaluated from TGA curves, decreases in the order S0 (75 %) \geq S1 (74.9 %) > S2 (63.1 %) > S3 (52.1 %) > S4 (43.9 %). These differences can be explained by the Si/K molar ratios, which decrease in the same order (Table 1). In fact, the increase in the amount of K_2O in the silicate solution promotes the formation of non-bridging oxygen. Consequently, the amount of water required during the manufacture of the corresponding geopolymers decreases.

Infrared spectroscopy was utilized to investigate the structure of each silicate solution. The infrared spectra recorded in the 4,000–1,400 cm^{-1} range are presented in Fig. 2Aa. Irrespective of the solution, the –OH and water bending vibrations are observed at approximately 3,300 and 1,650 cm^{-1} , respectively. The decrease in the intensities of these bands from S0 to S4 is in agreement with the

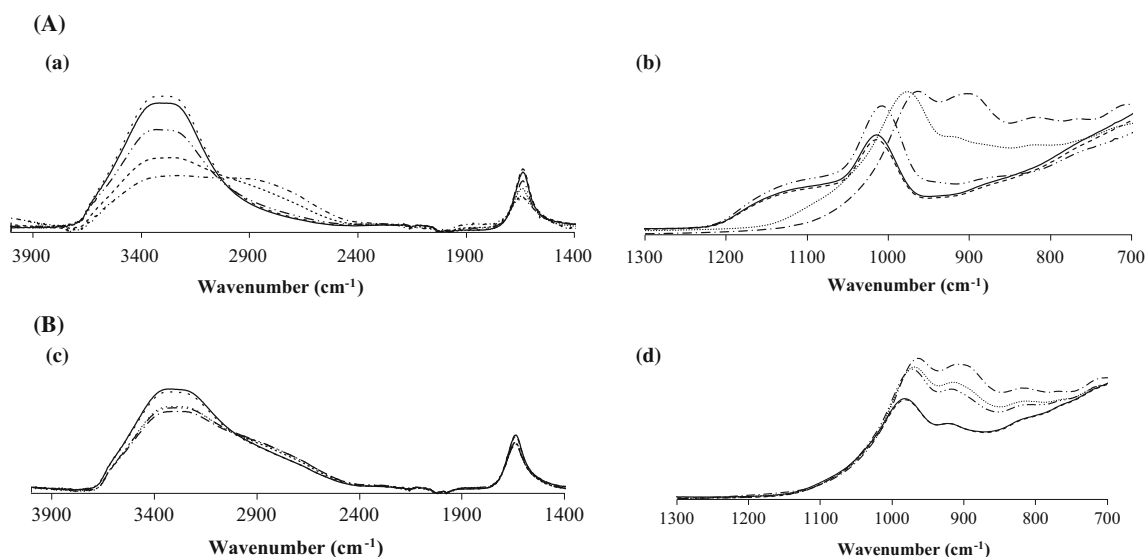


Fig. 2 FTIR spectra of (A) (a, b) (dashed line) S0, (solid line) S1, (line with double filled circle) S2, (filled circle) S3 and (line with single filled circle) S4 starting solutions and (B) (c, d) (dashed line)

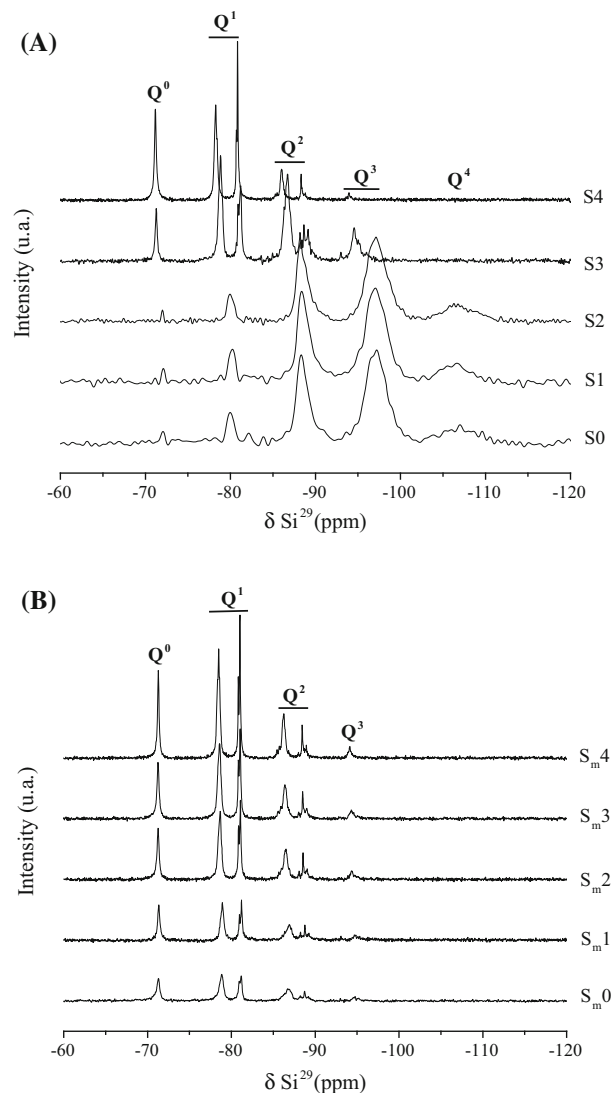
S_m0, (solid line) S_m1, (line with double filled circle) S_m2, (filled circle), S_m3 and (line with single filled circle) S_m4 modified solutions

Table 3 Main vibration bands of S0, S1, S2, S3, S4 starting silicate solutions

Band positions on silicate solutions spectra (cm ⁻¹)					Attribution
S0	S1	S2	S3	S4	
1,160	1,160	1,160	–	–	ν_{as} Si–O–Si (Q ⁴)
1,105	1,105	1,105	–	–	ν_{as} Si–O–Si (Q ³)
1,010	1,010	1,008	976	962	ν_{as} Si–O–Si (Q ²)
–	–	–	918	900	ν_{as} Si–O–Si (Q ¹)
–	–	–	820	976	ν_{as} Si–O–Si (Q ⁰)

previously discussed thermal analysis results. These differences primarily suggest that the silicate solutions have variable compositions in terms of siliceous species. Figure 2Ab presents the infrared spectra of the solutions in the 1,300–700 cm⁻¹ range to focus on the Qⁿ contributions of the siliceous species. The bands and their assignments are detailed in Table 3. The characteristic vibration bands of the Si–O–Si bond are located at approximately 1,200–1,000 cm⁻¹ [21]. A comparison between the spectra provides evidence of the presence of various silicon environments. For the S0 and S1 solutions, the bands at 1,160, 1,105 and 1,010 cm⁻¹ are asymmetric stretching vibrations characteristic of Si–O–Si (Q⁴), Si–O–Si (Q³) and Si–O–Si (Q²), respectively [19]. The S2 spectrum exhibits a similar trend, with a slight shift to lower wavenumbers. In the case of the S3 and S4 solutions, only bands with characteristics of ν_{as} Si–O–Si (Q²), ν_{as} Si–O–Si (Q¹) and ν_{as} Si–O–Si (Q⁰) at approximately 976, 916 and 819 cm⁻¹, respectively, are observed. The Q¹ and Q⁰ contributions appear to be more intense in the case of the S4 solution. Therefore, a decrease in the Si/K molar ratio of the silicate solution (Table 1) induces an increase in the formation of lower-order siliceous species (Q¹ and Q⁰) to the detriment of higher-order species (Q⁴, Q³ and Q²) [22].

The most efficient technique for providing additional details about the molecular structure is ²⁹Si MAS-NMR. The ²⁹Si NMR spectra of the starting solutions are plotted in Fig. 3a. The shifts at -72, -80, -88, -97 and -106 ppm are assigned to Q⁰, Q¹, Q², Q³ and Q⁴, respectively [23]. Broad bands associated with Q⁴, Q³ and Q² species are observed in the spectra of the S0, S1 and S2 solutions. The broad peaks are mainly due to a continuous range in the number of bridging oxygen atoms, with distorted sites having bonding characteristics between those of the well-defined tetrahedra in a silicate crystal [24]. In the S3 and S4 solutions, Q², Q¹ and Q⁰ predominate, whereas Q⁴ is totally absent. Furthermore, the appearance of Q² and Q¹ cyclic species are observed [25]. Thus, the ²⁹Si NMR results indicate that the S0, S1 and S2 solutions are similar in structure and contain condensed siliceous species.

**Fig. 3** Spectra of ²⁹Si MAS-NMR of (A) S0, S1, S2, S3 and S4 starting solutions and (B) S_m0, S_m1, S_m2, S_m3 and S_m4 modified solutions

However, the S3 and S4 solutions appear to be more depolymerized in comparison with the other solutions.

To confirm the thermal data, the amount of water in each solution, as estimated from the TGA analyses, is plotted as a function of the intensity ratio of the Q²/Q³ contributions determined by NMR and the number of non-bridging oxygen per tetrahedra (i.e., the NBO/T ratio), as calculated from the chemical composition of the starting solutions (NBO/T = (2 × K₂O)/SiO₂) [26] (Fig. 4). As expected, the amount of water in the silicate solution decreases with an increase in depolymerized species (i.e., at a high Q²/Q³ ratio) following an increase of non-bridging oxygen.

In summary, the existence of several contributions to the Si–O–Si band in the silicate solutions can be linked to the Si/K molar ratio of the solution. In fact, as the Si/K ratio decreases, the solution becomes more depolymerized.

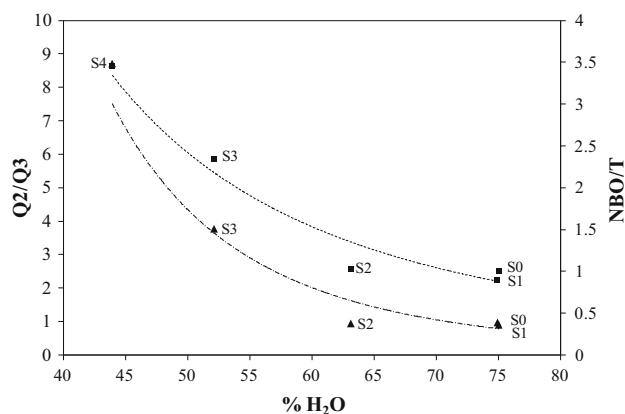


Fig. 4 Evolution of the amount of water, estimated from TGA analysis, in function of (filled triangle) the intensity ratio of the contributions Q^2/Q^3 determined by NMR and (filled square) the calculated number of non bridging oxygen per tetrahedra (NBO/T) for each starting solution

These results are in agreement with those obtained by Autef et al. [21], who studied different solutions prepared with various Si/K ratios by dissolution of amorphous silica in an alkali solution (water + KOH). The differences in terms of siliceous species and the degree of depolymerization between silicate solutions will induce different reactivities.

3.2 Modified solutions

A similar characterization was performed on the modified solutions ($S_{m0} \rightarrow S_{m4}$). The DTA–TGA curves, plotted in Fig. 1b, show similar profiles and highlight few changes compared to the curves of the starting solutions. The same endothermic phenomena (I, II, IV) previously discussed are distinguished, except for the third peak at 115 °C (III), which is very weak and close to nonexistent. The intensities of the peaks and the weight loss were accompanied by decreases [S_{m0} (66.2 %), S_{m1} (67.0 %), S_{m2} (53.4 %), S_{m3} (52.1 %)]. These changes reveal that the addition of KOH in S_0 , S_1 , S_2 and S_3 causes dissociation of colloids that were initially present in the solution, which induces water consumption [27]. Hence, a smaller amount of water is released from the solutions. The trends in the heat-flow and weight-loss curves of S_{m4} are the same as those observed for S_4 because KOH was not added to the S_4 solution. Solution S_{m4} is already depolymerized because of its large amount of K_2O .

The infrared spectra of the modified solutions (Fig. 2B) show similar profiles. The relative absorbance of the νOH ($3,300\text{ cm}^{-1}$) and δH_2O ($1,650\text{ cm}^{-1}$) bands in the spectra of the S_{m0} and S_{m1} samples are slightly more intense than those in the spectra of the other solutions (Fig. 2Bc). This fact can be explained by the large amount of water in the

S_0 and S_1 starting solutions. Furthermore, the decrease in the absorbance intensities relative to those observed in the spectra of the starting solutions (Fig. 2Bc) confirms the results obtained from thermal analysis (see below). At the same time, for the S_{m0} , S_{m1} and S_{m2} modified solutions, the band characteristic of asymmetric stretching vibrations of Si–O–Si (Q^4) disappeared, the band characteristic of Si–O–Si (Q^2) shifted from $1,015$ to 980 cm^{-1} and new bands related to Si–O–Si (Q^1) and Si–O–Si (Q^0) appeared. In the case of the spectrum of S_{m3} , the band intensities of Si–O–Si (Q^1) and Si–O–Si (Q^0) increased compared to those in the spectrum of S_3 . Finally, the IR spectrum profile of S_{m4} was the same as that of S_4 . Therefore, the nucleophilic attack by KOH breaks the Si–O–Si bonds to form Si–O–K bonds, which leads to the formation of non-bridging oxygen atoms and depolymerizes the solution [28].

To further assess the effect of the addition of KOH to the starting solutions, ^{29}Si NMR analysis was performed (Fig. 3b). The data highlight similarities between the siliceous species present in the modified solutions. Compared with the spectra of the initial solutions, those of the modified solutions exhibit narrower peaks, reflecting less distorted networks. The disappearance of the Q^4 species was also observed, as well as a strong decrease in the amount of Q^3 species and the appearance of Q^2 and Q^1 cyclic species, especially in the cases of S_{m0} , S_{m1} and S_{m2} .

In conclusion, the type of siliceous species present in a potassium silicate solution depends on the Si/K ratio. Upon the addition of KOH, the bonds between the condensed silicon species in the initial silicate solution are destroyed. Hence, the amounts of potassium ions and free silicate species increase, leading to the formation of lower-order species, which are more reactive, as previously reported by Liabau [29].

3.3 Mixtures of alkaline solutions and metakaolin

To exacerbate the reactivity of the siliceous species present in the different alkaline solutions, five reactive mixtures were prepared using the same metakaolin M-1000. The structural evolution of the mixtures was followed by FTIR in ATR mode. Figure 5 shows the Q^2 shift as a function of time for the different mixtures. The evolution of the position of this band, located at approximately 980 cm^{-1} , indicates the substitution of Si–O–Si by Si–O–Al bonds and thereby reflects the reorganization of the network due to a geopolymerization reaction [8]. In addition, the slope of the curve in the beginning of the reaction is characteristic of the kinetics of this substitution [8]. For all samples, the position of the Q^2 band shifted toward lower wavenumbers over time. The initial band positions were similar for G_0 (983 cm^{-1}) and G_1 (984 cm^{-1}) and lower for G_2 (972 cm^{-1}), G_3 (970 cm^{-1}) and G_4 (964 cm^{-1}). This fact

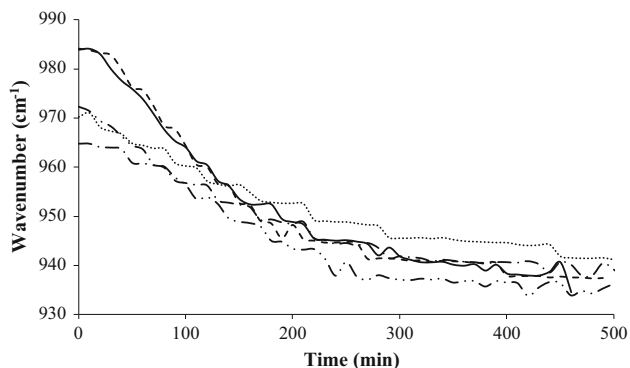


Fig. 5 Shift of Q^2 position from IR spectra versus the time (dashed line) G 0, (solid line) G1, (line with double filled circle) G2, (filled circle) G3 and (line with single filled circle) G4 reactive mixtures

can be explained by the presence of different amounts of non-bridging oxygen, which results in different extents of depolymerization between the alkali solutions despite the solutions having the same Si/K molar ratio.

The shift and the slope values for the five samples are reported in Table 4. These values are characteristic of aluminosilicate network formation. According to previous work [30], M-1000 is not pure metakaolin because of the presence of silicates such as quartz and mica. Moreover, the presence of these phases induces the combination of Si–O–M (M = Si, Al or K) from dissolved species and from the impurities of metakaolin. The IR spectra of the G0 and G1 geopolymer samples exhibit the greatest shift and slope values (shifts of 46 and 49 cm^{-1} , respectively; see Table 4). However, G2, G3 and G4 exhibit smaller slope and shift values, indicating differences between the networks formed in each sample. These differences may influence the working properties of the materials. To verify this hypothesis, the mechanical properties of the five consolidated materials were evaluated by subjecting the samples to compression for 7 days. The results are presented in Fig. 6. The materials exhibited compressive strength values greater than 32 MPa. The G3 sample exhibited the highest mechanical strength (approximately 60 MPa), followed by G4 (56 MPa) and G2 (50 MPa), whereas G0 and G1 exhibited the lowest compressive strengths (32 and

Table 4 Values of the shift and the slope obtained by infrared spectroscopy for each sample

Sample	Shift (cm^{-1})	Slope ($\text{cm}^{-1}/\text{min}$)
G0	46	-0.21
G1	49	-0.21
G2	38	-0.14
G3	29	-0.09
G4	26	-0.09

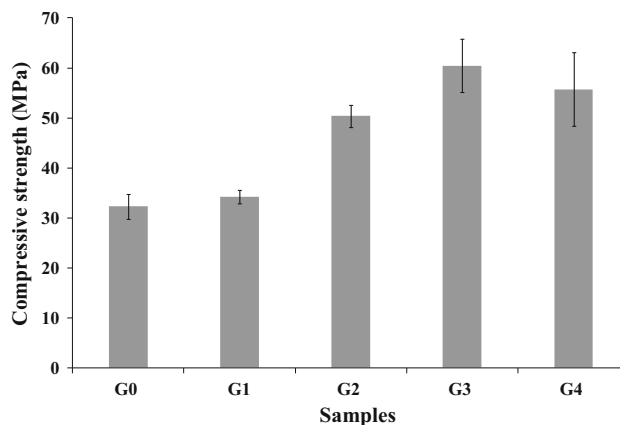


Fig. 6 Compressive strength of each sample after 7 days of ageing

34 MPa, respectively). These results confirm the trends observed in the FTIR spectra.

3.4 Relationship between working properties of geopolymers and reactivity of the alkaline solutions

To correlate the mechanical properties of the geopolymers with the reactivity of the different solution compositions, the compressive strength values of the geopolymers were plotted as functions of the slopes obtained from the FTIR spectra (Fig. 7). The results show a relationship ($R^2 = 0.97$) between these two parameters. In fact, the smaller slopes observed in the spectra of the G3 and G4 samples indicate the slow kinetics of the Si–O–Si bond substitution by Si–O–Al, and these samples exhibit the best mechanical properties among the investigated samples. We obtained similar results in our previous work [30] on the role of metakaolin precursors, where we used highly

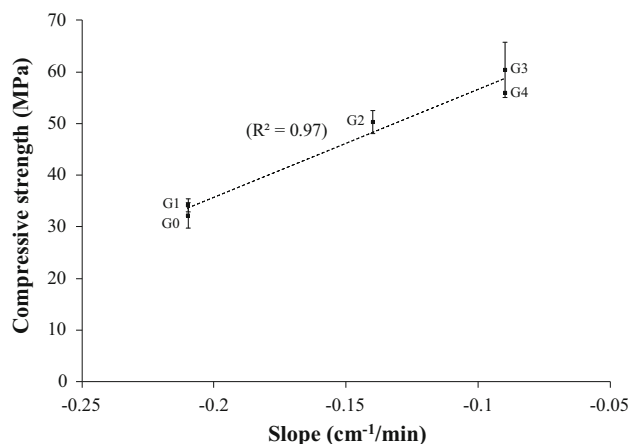


Fig. 7 Relation between the compressive strength and the slope for each sample. The dash point (dashed line) represents the linear regression line with $R^2 = 0.97$

reactive metakaolin. In the amorphous phase, Si and Al react easily in an alkaline medium, resulting in a smaller shift and slope; however, this configuration exhibits the highest compressive strength. The quickly released siliceous species reach speciation equilibrium and then react with the aluminous species because of their high reactivity. This reaction leads to the formation of a perfect geopolymer network, which enhances the mechanical properties of the final materials.

To more thoroughly evaluate this evolution, the compressive strength as well as the slope were plotted as functions of the ratio of intensities $\left[\frac{(Q^2/Q^3_{\text{modified solutions}})}{(Q^2/Q^3_{\text{starting solutions}})} \right]$ determined by ^{29}Si MAS-NMR. These plots reveal the influence of the extent of depolymerization of the starting solutions (Fig. 8). Two linear relationships are shown. For the lower $\left[\frac{(Q^2/Q^3_{\text{modified solutions}})}{(Q^2/Q^3_{\text{starting solutions}})} \right]$ ratios, better mechanical strengths and smaller slopes were observed, especially in the case of G2, G3 and G4. Indeed, the abundance of low-order species (Q^2 in this case) and, consequently, more extensively depolymerized starting solutions increases the reactivity of the mixture and leads to the rapid formation of small colloids that aggregate more rapidly to form the network [23].

The data suggest that correlation of the working properties and the reactivity of the mixtures to the chemical composition of the different synthesized materials is useful. Figure 9 presents the evolution of the compressive strength and the shift in the ratio $(n\text{Si} \cdot n\text{H}_2\text{O})/(n\text{K} + n\text{Al})$. Typically, the compressive strength decreased with increasing $(n\text{Si} \cdot n\text{H}_2\text{O})/(n\text{K} + n\text{Al})$, whereas the shift increased. The silicon and potassium availabilities differ between the five mixtures, which led to the variation in reactivity and,

consequently, to the formation of various networks [31]. The G0 and G1 compositions are silicon-rich, which explains the amount of gel phase observed during the synthesis. In fact, an excess of siliceous species leads to polymerization and thus to the formation of a gel [32]. Competition between a Si-rich phase (gel) and a geopolymer phase weakened the structure. According to the literature [33], the mechanical properties of geopolymers depends on their water content. The large amounts of water in G0 and G1, which resulted from the high water content in the starting silicate solutions (S0 and S1, see Table 1), results in a greater amount of trapped water, which may also explain the comparatively worse compressive strengths of these samples. In the case of G2, G3 and G4, the larger amount of potassium and the accentuated presence of depolymerized species in the alkaline solution (Tables 1, 2) led to the formation of small, very reactive entities that quickly bridge Si and/or Al. This fact explains their relatively weak shift values and reveals the presence of two imbricated networks, which lead to an improvement in the mechanical strength of these samples. These explanations were validated by TEM investigations to provide additional structural information. The TEM micrographs of both compositions are presented in Fig. 10. They clearly highlight the differences in morphology between the G1 and G3 samples. Sample G3 contains smaller entities than sample G1, which confirms the previously discussed hypothesis. In summary, the extent of depolymerization of the activation solution and the chemical composition of the mixture are critical parameters that lead to nanostructural variations and govern the mechanical properties of the resulting geopolymers.

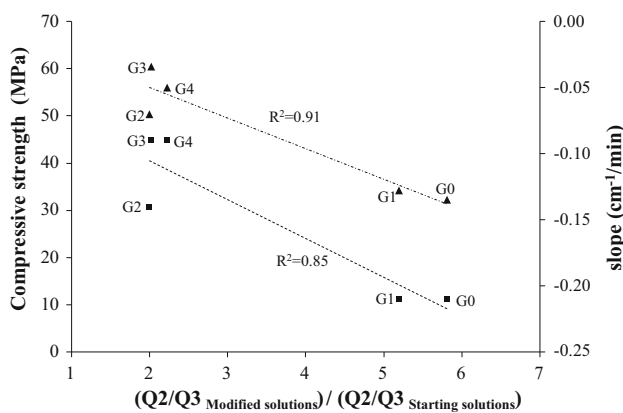


Fig. 8 Evolution of (filled triangle) the compressive strength and (filled square) the slope in function of the ratio of intensity $\left[\frac{(Q^2/Q^3_{\text{modified solutions}})}{(Q^2/Q^3_{\text{starting solutions}})} \right]$ determined by ^{29}Si MAS-NMR for each mixture

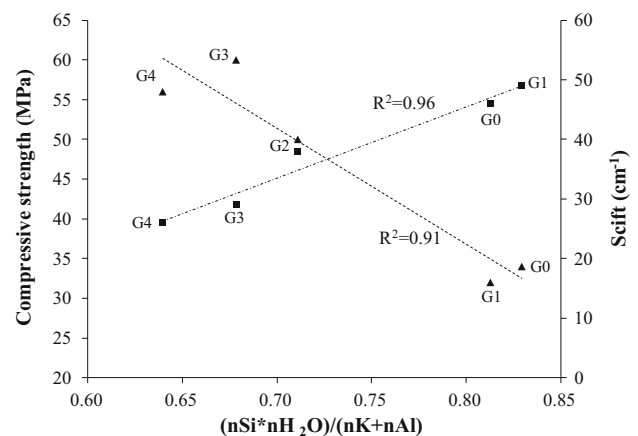


Fig. 9 Evolution of (filled triangle) the compressive strength and (filled square) the shift in function of the chemical compositions $(n\text{Si} \cdot n\text{H}_2\text{O})/(n\text{K} + n\text{Al})$ of each mixture

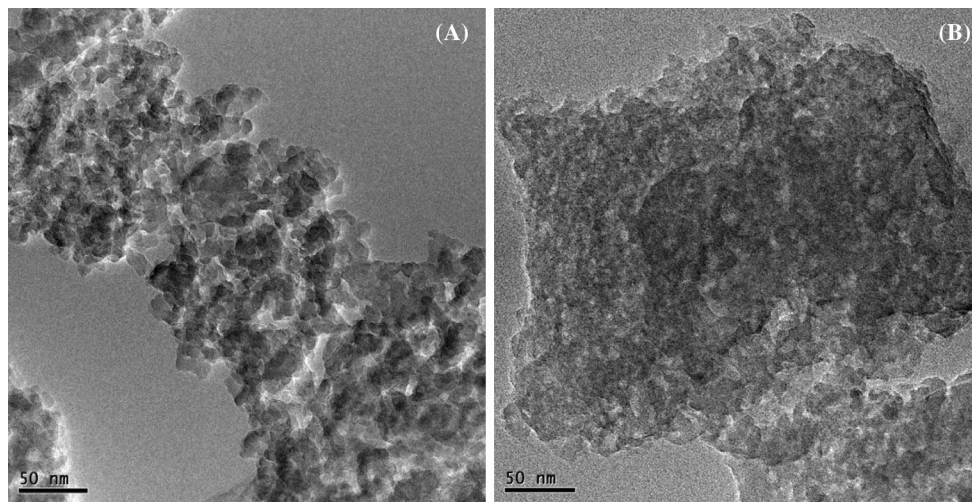


Fig. 10 TEM micrographs of (A) G1 and (B) G3 samples

4 Conclusion

Our elucidation of the geopolymerization reaction involved a comprehensive study of the precursors used. In the present work, the influence of the activating solution was demonstrated. Indeed, the Si/K ratio was observed to control the degree of depolymerization of the silicate solutions as well as the type and the amount of the siliceous species. Moreover, a relationship between the compressive strengths of geopolymers, the kinetics of Si–O–Si bond substitution by Si–O–Al, the chemical composition and the type of siliceous species in the alkaline solutions was demonstrated. In conclusion, depolymerized species are small and highly reactive, which enables the fast formation of oligomers and leads to better mechanical properties of the resulting geopolymers.

References

1. Van Jaarsveld JGS, Van Deventer JSJ, Lorenzen L (1999) The potential use of geopolymeric materials to immobilise toxic metals: part I Theory and applications. *Miner Eng* 10:659–669
2. Krivenko P (1997) Alkaline cements: terminology, classification, aspects of durability [C] Proceedings of the 10th International Congress on the Chemistry of Cement, Gothenburg, Sweden
3. Liew YM, Kamarudin H, Mustafa Al Bakri AM, Luqman M, Khairul Nizar I, Heah CY (2011) Investigating the possibility of utilization of kaolin and the potential of metakaolin to produce green cement for construction purposes. *Aust J Basic Appl Sci* 5:441–449
4. Davidovits J (2008) *Geopolymer: Chemistry and Applications*, 2nd edn. Institut Géopolymère, St-Quentin
5. Zibouche F, Kerdjoudj H, d'Espinose de Lacaillerie JB, Van Damme H (2009) Geopolymers from Algerian metakaolin. Influence of secondary minerals. *Appl Clay Sci* 43:453–458
6. Elimbi A, Tchakoute KH, Njopwouo D (2011) Effects of calcination temperature of kaolinite clays on the properties of geopolymer cements. *Constr Build Mater* 25:2805–2812
7. Zhang YJ, Li S, Wang YC, Xu DL (2012) Microstructural and strength evolutions of geopolymer composite reinforced by resin exposed to elevated temperature. *J Non Cryst Solids* 358:620–624
8. Autef A, Joussein E, Poulesquen A, Gasgnier G, Pronier S, Sobrados I, Sanz J, Rossignol S (2013) Influence of metakaolin purities on potassium geopolymer formulation: the existence of several networks. *J Colloids Interface Sci* 408:43–53
9. Duxson P, Provis JL, Lukey GC, Mallicoate SW, Kriven WM (2005) Understanding the relationship between geopolymer composition, microstructure and mechanical properties. *Colloids Surf A* 269:47–58
10. Duxson P, Fernandez-Jimenez A, Provis JL, Lukey GC, Palomo A, Van Deventer JSJ (2007) The effect of alkali and Si/Al ratio on the development of mechanical properties of metakaolin-based geopolymers. *J Mater Sci* 42:2917–2933
11. Swaddle TW (2001) Silicate complexes of aluminum (III) in aqueous systems. *Coord Chem Rev* 219:665–686
12. Engelhard G, Zeigan D, Jancke H, Hoebbel D, Weiker Z (1975) High resolution ^{29}Si NMR of silicates and Zeolites. *Anorg Allg Chem* 418:17–28
13. MacDonald SA, Schardt CR, Masiello DJ (2000) Dispersion analysis of FTIR reflection measurements in silicate glasses. *J Non Cryst Solids* 275:72–82
14. Matson W, Sharma SK, Philpotts JA (1983) The structure of high silica alkali-silicate glasses. A Raman spectroscopic investigation. *J Non Cryst Solids* 58:323–352
15. Prud'homme E, Michaud P, Joussein E, Clacens JM, Rossignol S (2011) Role of alkaline cations and water content on geomaterial foams: monitoring during formation. *J Non Cryst Solids* 357:1270–1278
16. ASTM D1633 – 00, Standard test methods for compressive strength of molded soil cement cylinders, 2007
17. Haynes WM (2013) *CRC handbook of chemistry and physics*, 94th edn. CRC Press, Boca Raton, Florida
18. Langille KB, Nguyen D, Bernet JO, Veinot DE (1991) Mechanism of dehydration and intumescence of soluble silicates. I, Effect of silica to metal oxide molar ratio. *J Mater Sci* 26:695–703
19. Prud'homme E, Michaud P, Joussein E, Smith A, Peyratout C, Sobrados I, Sanz J, Rossignol S (2012) Geomaterial foams: role

- assignment of raw materials in the network formation. *J Sol-Gel Sci Technol* 61(2):436–448
20. Jonathan LB, Garry LT (1997) Anion distributions in sodium silicate solutions. Characterization by ^{29}Si NMR and infrared spectroscopies, and vapor phase osmometry. *J Phys Chem B* 101:10638–10644
 21. Autef A, Joussein E, Gasgnier G, Rossignol S (2013) Role of the silica source on the geopolymerization rate: a thermal analysis study. *Ceram Eng Sci Proc* 33:13–24
 22. Goudarzi N (2013) Silicon-29 NMR spectroscopy study of the effect of tetraphenylammonium (TPA) as a template on distribution of silicate species on alkaline aqueous and alcoholic silicate solutions. *Appl Magn Reson* 44:469–478
 23. Prud'homme E, Autef A, Essaidi N, Michaud F, Samet B, Joussein E, Rossignol S (2013) Defining existence domains in geopolymers through their physicochemical properties. *Appl Clay Sci* 73:26–34
 24. Schmidt BC, Riemer T, Kohn SC, Holtz F (2001) Structural implications of water dissolution in haplogranitic glasses from NMR spectroscopy: influence of total water content and mixed alkali effect. *Geochim Cosmochimi Acta* 65:2949–2964
 25. Wijnen PWJG, Beelen JW, Rummens CPJ, Van de Ven LJM, Van Santen RA (1989) Silica gel dissolution in aqueous alkali metal hydroxides studies by ^{29}Si -Nmr. *J Non Cryst Solids* 109:85–94
 26. Halter WE, Morizet Y, Meier BH, Verel R (2007) Structural control on bulk melt properties: single and Double quantum ^{29}Si NMR spectroscopy on alkali-silicate glasses. *Geochim Cosmochimi Acta* 71:6002–6018
 27. Schneider E, Stebbins JF, Pines A (1987) Speciation and local-structure in alkali and alkaline-earth silicate-glasses-constraints from Si-29 NMR-spectroscopy. *J Non Cryst Solids* 89:371–383
 28. Bunker BC, Tallant DR, Headley TJ, Turner GL, Kirkpatrick R (1988) Structure of leached sodium borosilicate glass. *Phys Chem Glasses* 29:106
 29. Liebau F (1985) Structural chemistry of silicates. Springer, Berlin
 30. Autef A, Joussein E, Poulesquen A, Gasgnier G, Pronier S, Sobrados I, Sanz J, Rossignol S (2013) Role of metakaolin dehydroxylation in geopolymer synthesis. *Powder Technol* 250:33–39
 31. Hajimohammadi A, Provis JL, Van Deventer JSJ (2011) The effect of silica availability on the mechanism of geopolymerisation. *Cem Concr Res* 41:210–216
 32. Autef A, Prud'homme E, Joussein E, Gasgnier G, Pronier S, Rossignol S (2013) Evidence of a gel in geopolymer compounds from pure metakaolin. *J Sol-Gel Sci Technol* 65:220–229
 33. Steveson M, Sagoe-Crentsil K (2005) Relationships between composition, structure and strength of inorganic polymers. *J Mater Sci* 40:2023–2036